CONF-8706166--2

BNL--40074

DE87 014283

KAON-NUCLEUS REACTIONS AND HYPERNUCLEI

C. B. Dover
Physics Department
Brookhaven National Laboratory
Upton, NY 11973
U S A

ABSTRACT

Recent advances in hypernuclear physics and kaon-nucleus scattering are discussed, with emphasis on the spectroscopy of Λ single particle states in heavy systems, as revealed by the (π^+, K^+) reaction.

Invited Talk
International Symposium on Medium Energy Physics
Institute of High Energy Physics, Academia Sinica
Beijing, China
June 23-27, 1987

Kaon-Nucleus Reactions and Hypernuclei

C. B. Dover
Physics Department
Brookhaven National Laboratory
Upton, NY 11973
U S A

ABSTRACT

Recent advances in hypernuclear physics and kaon-nucleus scattering are discussed, with emphasis on the spectroscopy of Λ single particle states in heavy systems, as revealed by the (π^+, K^+) reaction.

1. HYPERNUCLEAR PHYSICS

Progress in the field of hypernuclear physics has been extensively reviewed in the Proceedings of two recent conferences[1,2]. There have been advances in several areas: weak decays of hypernuclei, searches for $S = -1$ dibaryons via the $d\left(K^-, \pi^-\right)\Lambda p$ reaction, spin splittings in Λ hypernuclei as measured in the $\left(K^-, \pi^-\gamma\right)$ process, and studies of Σ hypernuclei. There are excellent prospects for the future study of $S = -2$ dibaryons and hypernuclei via the $\left(K^-, K^+\right)$ reaction : a new high momentum (1-2 GeV/c) K^- beam line has recently been approved for the Brookhaven AGS.

Rather than attempting to review the whole field of hypernuclear physics in a cursory way, I refer the reader to Refs. [1,2] for previous work and focus attention on the interpretation of some very recent Brookhaven results[3] on the production of hypernuclei via the $\left(\pi^+, K^+\right)$ reaction.

1.1. Associated Production of Hypernuclei

The use of energetic pion beams for hypernuclear production was proposed by Dover, Ludeking and Walker[4], and further studied theoretically by Bando and collaborators[5]. The first demonstration that the method was experimentally practical was due to Milner et al[6], who studied the $^{12}C\left(\pi^+, K^+\right)\,^{12}_{\Lambda}C$ reaction at a

This work has been supported by the U. S. Department of Energy under contract no. DE-AC02-76CH00016.

lab momentum $p_\pi = 1.05$GeV/c. Very recently, the (π^+, K^+) reaction has been studied[3] with heavy targets, leading to the very interesting results on the A dependence of Λ binding energies to be discussed here.

First a short review of motivation. For the conventional (K^-, π^-) reaction,

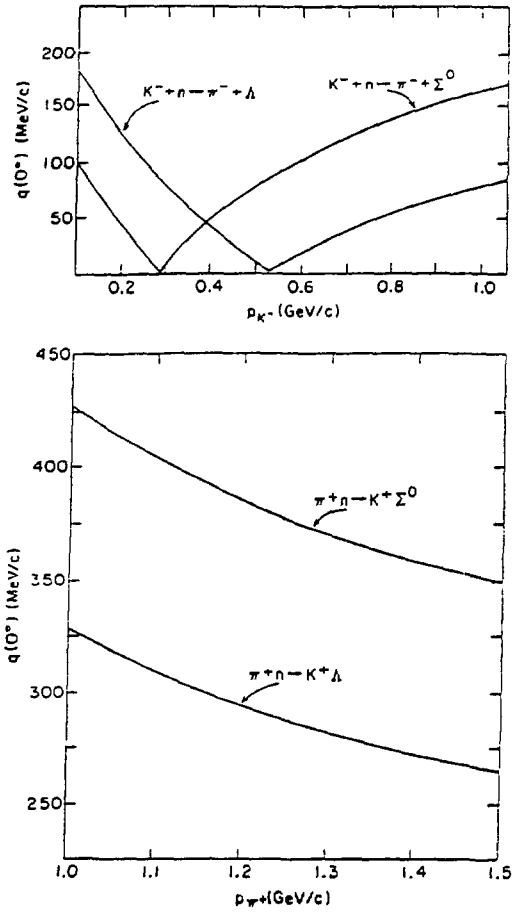

Fig. 1: The lab momentum transfer q at $\theta_L = 0°$ as a function of incident lab momentum for the processes $K^- + n \to \pi^- + \Lambda$, $\pi^- + \Sigma^0$ and $\pi^+ + n \to K^+ + \Lambda$, $K^+ + \Sigma^0$ on a heavy target nucleus. Many body kinematics is used to calculate q, neglecting binding energy changes and assuming the target to be at rest in the lab. (from ref. 4)

the momentum transfer q is zero for a "magic momentum" of about 530 MeV/c for Λ and 290 MeV/c for Σ^0 production, as shown in Fig. 1. This favors the formation of low spin "substitutional" states of the hypernucleus for small π^- angle θ_L.

The (π^+, K^+) reaction, on the other hand, is endoergic, so q remains larger than or equal to the Fermi momentum $p_F \approx 270 MeV/c$, for the entire region of pion momentum p_π for which the two-body $\pi^+ n \to K^+ \Lambda$ cross section remains sizable. The momentum dependence of this cross section is displayed in Fig. 2. Because of the substantial q in (π^+, K^+), even at $\Theta_L = 0°$, the production of high spin hypernuclear states is favored. Thus, the (π^+, K^+) and (K^-, π^-) reactions are complementary.

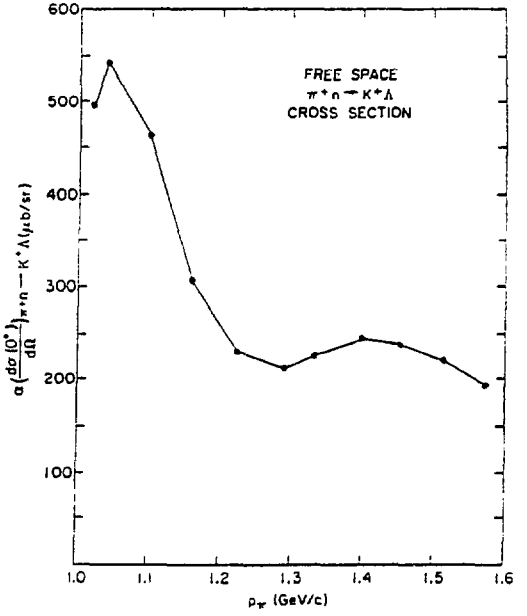

Fig. 2: Momentum dependence of the free space lab differential cross section at 0° for the $\pi^+ n \to K^+ \Lambda$ reaction. (from ref. 4)

Starting from a 0^+ target, the lab differential cross section for the excitations of a pure Λ particle-neutron hole (ph) configuration of spin-parity J^π in the (π^+, K^+) reaction is given by

$$\frac{d\sigma}{d\Omega}(0^+ \to J^\pi) = \alpha \left(\frac{d\sigma}{d\Omega}\right)_{0°}^{\pi^+ n \to K^+ \Lambda} N_{\text{eff}}^J \qquad (1)$$

where the two-body $\pi^+ n \to K^+ \Lambda$ lab cross section $\alpha\,(d\sigma/d\Omega)_{0°}$ is plotted in Fig. 2 and N_{eff}^J is the effective neutron number, which in the plane wave approximation (PWA) reads

$$N_{\text{eff}}^J = (2J+1)\,(2j_\Lambda + 1)\,(2j_n + 1) \begin{pmatrix} j_\Lambda & j_n & J \\ 1/2 & -1/2 & 0 \end{pmatrix}^2 F(q) \qquad (2)$$

with

$$F(q) = \left[\int_0^\infty r^2 dr\, R_\Lambda(r)\, R_n(r)\, j_J(qr)\right]^2 . \tag{3}$$

Here R_Λ and R_n are radial wave functions for the Λ and n single particle states $\{l_\Lambda, j_\Lambda\}$ and $\{l_n, j_n\}$, respectively. For (π^+, K^+), and for (K^-, π^-), the cross section for spin-flip is expected to be negligible, so only natural parity ph states will be populated. In $(e, e'K^+)$ or (γ, K^+), on the other hand,spin flip states will be strongly excited. Because of the high q for (π^+, K^+), the "stretch" configurations with $J = l_\Lambda + l_n$ will be kinematically favored. For transitions between nodeless n and Λ oscillator states, the form factor $F(q)$ for "stretch" states is given by

$$F(q) = \frac{(2Z)^J\, e^{-z}\, [\Gamma(J+3/2)]^2}{[(2J+1)!!]^2\, \Gamma(l_\Lambda + 3/2)\, \Gamma(l_n + 3/2)} \tag{4}$$

where $Z = (bq)^2/2$ and b is the oscillator radius parameter. A transition is optimally matched kinematically when $F(q)$ is maximum, i.e. when $dF(q)/dq = 0$ or

$$J = (bq)^2/2 . \tag{5}$$

In Fig. 3, we plot J, as given by Eq. (5), as a function of mass number A, using the relation

$$b \approx 0.96\, A^{1/3} \Big/ \left(1 - \frac{5}{9} A^{-1/3}\right)^{1/2} \tag{6}$$

obtained from $b^2 = \hbar/m_N\omega_N$, using the standard parametrization $\hbar\omega_N \approx 45\, A^{-1/3} - 25\, A^{-2/3}$. We see that at $p_\pi = 1.05$GeV/c, there is good kinematic matching for the high spin members of the "leading trajectory" where the Λ in $\{s_\Lambda, p_\Lambda, d_\Lambda \ldots\}$ single particle orbits is coupled to a neutron hole in the last valence shell. The state of maximum cross section (for fixed Z) is found to have J close to (within one unit of spin) the value given by Eq. (5). As a specific example, consider ^{90}Zr (π^+, K^+) $^{90}_{\Lambda}$Zr at $p_\pi = 1.05$GeV/c, where $Z \approx 6.2$ (using $q = 320$MeV/c and b from Eq. (6)). For the $\left(l_\Lambda \times g_{9/2}^{-1}\right)_{J=l_\Lambda+4}$ band, we find

$$N_{\rm eff}^J = \begin{cases} 10Z^4 e^{-z}/945 & \text{(J=4)} \\ 10Z^5 e^{-z}/1701 & \text{(J=5)} \\ 10Z^6 e^{-z}/6237 & \text{(J=6)} \\ 10Z^7 e^{-z}/34749 & \text{(J=7)} \\ 4Z^8 e^{-z}/104247 & \text{(J=8)} \end{cases} \tag{7}$$

where we have summed over $j_\Lambda = l_\Lambda \pm 1/2$. This leads to the cross sections listed in Table 1. Note that the peak cross section is for the $\left(f_\Lambda \times g_{9/2}^{-1}\right)_{7^-}$ state, but

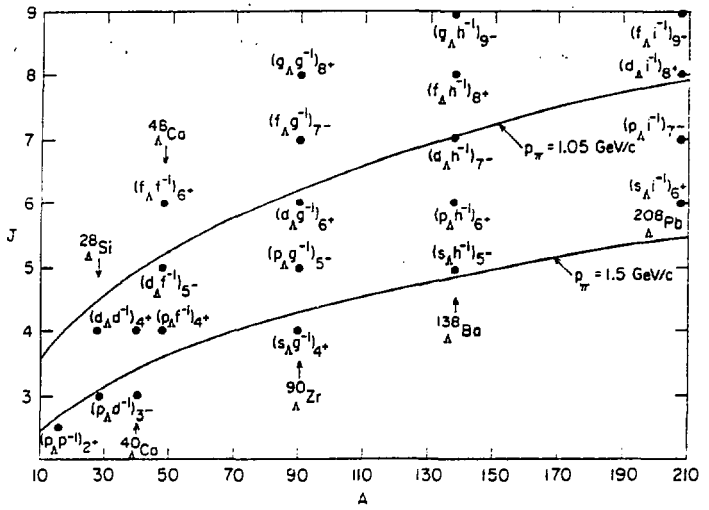

Fig. 3: Kinematically matched J values [Eq. (5)] as a function of A for pion lab momentum $p_\pi = 1.05$GeV/c and 1.5GeV/c are shown as solid lines. Typical natural parity Λn^{-1} states with $J = \ell_\Lambda + \ell_n$ are also shown for selected cases.

the 6^+ cross section is only slightly smaller. From Fig. 3, we see that both these states have $F(q)$ near its maximum value, so these transitions to high spin states are highly favored. In Table 1, we also show the PWA cross sections to "stretch" states $\left(l_\Lambda \times f^{-1}\right)_{J=l_\Lambda+3}$ involving the more deeply bound $f_{5/2}$ and $f_{7/2}$ neutron orbits. The excitation energies are estimated by using binding energies of 10.5, 14.3, and 18.5 MeV for the $g_{9/2}$, $f_{5/2}$ and $f_{7/2}$ neutron orbits, respectively, taken from Fig. 2.30 of Bohr and Mottelson[7] and Λ excitation energies (relative to s_Λ) of $\{6.5, 13.5, 21, 29$ MeV$\}$ for $\{p_\Lambda, d_\Lambda, f_\Lambda, g_\Lambda\}$, respectively, taken directly from the experimental data on ^{89}Y (π^+, K^+) $^{89}_{\Lambda}$Y (see later).

The configurations shown in Table 1 are expected to provide the largest contribution to the (π^+, K^+) cross section, because of their high spins, although numerous other ph configurations of low spin also exist, these becoming rather dense at higher excitation energy. Note that the $\left(\ell_\Lambda \times g_{9/2}^{-1}\right)$ states clearly dominate up to about 15 MeV excitation, whereas above 15 MeV the f^{-1} strength in PWA is comparable or even larger. In Table 1, distortion effects are neglected: absorption is expected[4] to reduce the PWA estimates considerably, more so for

Table 1

Cross sections in PWA for ^{90}Zr (π^+, K^+) $^{90}_{\Lambda}$Zr at 1.05 GeV/c

State	Excitation Energy (MeV)	$(d\sigma/d\Omega)_{L,0^o}$ $(\mu b/sr)$
$\left(s_\Lambda \times g_{9/2}^{-1}\right)_{4^+}$	0	12.7
$\left(s_\Lambda \times f_{5/2}^{-1}\right)_{3^-}$	3.8	11.1
$\left(p_\Lambda \times g_{9/2}^{-1}\right)_{5^-}$	6.5	43.8
$\left(s_\Lambda \times f_{7/2}^{-1}\right)_{3^-}$	8.0	14.8
$\left(p_\Lambda \times f_{5/2}^{-1}\right)_{4^+}$	10.3	39.3
$\left(d_\Lambda \times g_{9/2}^{-1}\right)_{6^+}$	13.5	74.0
$\left(p_\Lambda \times f_{7/2}^{-1}\right)_{4^+}$	14.5	52.4
$\left(d_\Lambda \times f_{5/2}^{-1}\right)_{5^-}$	17.3	82.4
$\left(f_\Lambda \times g_{9/2}^{-1}\right)_{7^-}$	21.0	82.0
$\left(d_\Lambda \times f_{7/2}^{-1}\right)_{5^-}$	21.5	110.0
$\left(f_\Lambda \times f_{5/2}^{-1}\right)_{6^+}$	24.8	110.0
$\left(g_\Lambda \times g_{9/2}^{-1}\right)_{8^+}$	29.0	68.0
$\left(f_\Lambda \times f_{7/2}^{-1}\right)_{6^+}$	29.0	146.4

states of lower J. The data of Chrien et al[3] suggest a cross section of $0.7\mu b/sr$ for the ground state of $^{89}_{\Lambda}$Y, an absorption factor of 18 with respect to Table 1.

Another effect which is important is the fragmentation of single particle states, which spreads the ph strength over more complicated configurations. This becomes more important as the binding energy of the neutron orbit increases, and would tend to disperse the $\left(\ell_\Lambda \times f^{-1}\right)$ strength into a smooth "background." Even though this "background" is sizable, and grows with increasing excitation energy, it is not strongly peaked. One can still assume that the sharp structures seen in the (π^+, K^+) spectrum are due predominantly to $\left(\ell_\Lambda \times g_{9/2}^{-1}\right)_{J=\ell_\Lambda+4}$ strength, and the peak energies can be used to obtain the Λ binding energies in various ℓ_Λ states. The effects of π^+ and K^+ optical distortions and the fragmentation

of single particle strength are under investigation by the Brookhaven group, and must be included in a quantitative analysis.

1.2 The Brookhaven (π^+, K^+) Data

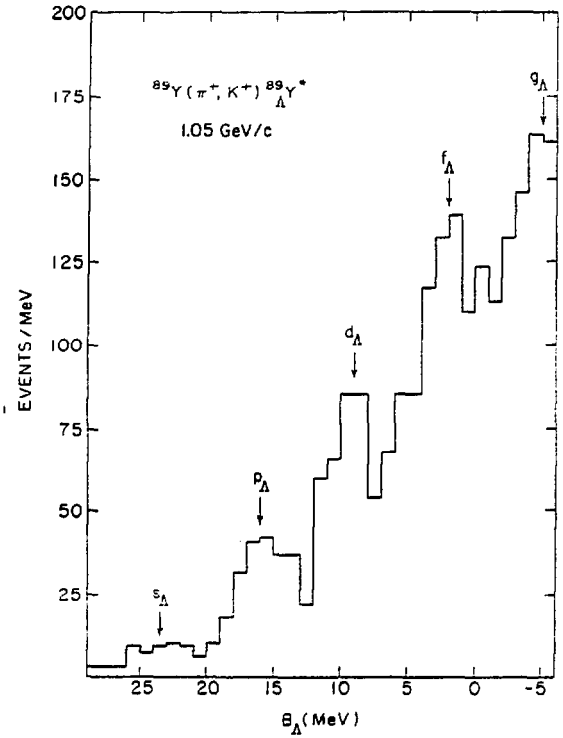

Fig. 4: The excitation spectrum of the $^{89}_{\Lambda}$Y* hypernucleus, as produced in the (π^+, K^+) reaction at 1.05 GeV/c. The data are taken from ref. 3. B_Λ is the binding energy of the Λ, here defined to be positive for bound states. The labels $\{s_\Lambda, p_\Lambda, d_\Lambda, f_\Lambda, g_\Lambda\}$ identify the values of B_Λ predicted in ref. 4 based on a Woods-Saxon potential for the Λ.

Recently, a Brookhaven–LANL–Houston–Tohoku–TRIUMF–Vassar– CMU–FSU–Mississippi collaboration has measured[3] (π^+, K^+) cross sections on ^{9}Be, ^{12}C, ^{13}C, ^{16}O, ^{28}Si, ^{40}Ca, ^{51}V, and ^{89}Y targets at $p_\pi = 1.05$GeV/c. These represent the first data for heavy targets, and enable us to track the evolution of Λ single particle binding energies as a function of A. The data for ^{89}Y (π^+, K^+) $^{89}_{\Lambda}$Y are shown in Fig. 4. One observes a series of rather sharp peaks on a smoothly rising background. We identify these peaks with the $s_\Lambda, p_\Lambda, d_\Lambda$, and f_Λ bound states of the Λ. The arrows in Fig. 4 indicate the orbital angular momenta assigned to these

states. These energies are very close to those predicted by Dover, Ludeking and Walker[4] as Λ bound states in a Woods-Saxon single particle potential $V_\Lambda(r)$ of the Λ of the form

$$V_\Lambda(r) = -V_0 \Big/ \left(1 + e^{(r-R)/a}\right) \tag{8}$$

with $V_0 = 30.7$ MeV, $R = r_0 A^{1/3}$, $r_0 = 1.1$ fm, and $a = 0.6$ fm. The full set of s_Λ, p_Λ, and d_Λ binding energies predicted[4] are shown as triangles in Fig. 5, where we also plot the observed binding energies B_Λ of Chrien et al[3] as a function of A.

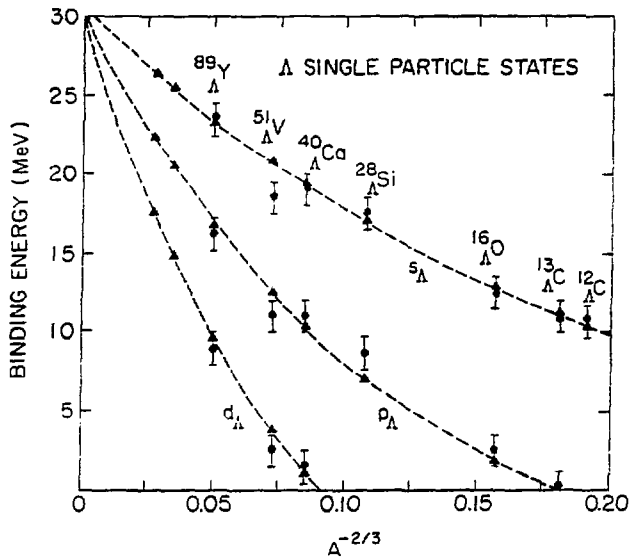

Fig. 5: The experimental binding energies of the s_Λ, p_Λ, and d_Λ states as a function of $A^{-2/3}$ are plotted as solid circles. The triangles represent the predictions of ref. 4, based on the Woods-Saxon potential of Eq. (8). The dashed line is drawn through the Woods-Saxon predictions.

Note that the nodeless g_Λ state is predicted[4] to lie about 5 MeV in the continuum near $A = 90$, with an elastic width of about 900 keV, and may be visible in the data. This width is small because of the relatively large ℓ_Λ of the state. The existence of a narrow single particle Λ resonance in the continuum is not specific to the mass 90 region. Narrow states ($1d_\Lambda$ in ${}^{28}_{\Lambda}$Si, $1h_\Lambda$ in ${}^{138}_{\Lambda}$Ba, $1i_\Lambda$ in ${}^{208}_{\Lambda}$Pb, for instance) with elastic widths of 1 MeV or less are predicted throughout the periodic table.

Note that we regard the ${}^{89}_{\Lambda}$Y and ${}^{90}_{\Lambda}$Zr cases as containing essentially the same information on Λ single particle energies. This is justified, since the $2P^{-1}_{1/2}$ proton

hole plays little role in the energetics. The spin splittings of the hypernuclear levels with $j_\Lambda = \ell_\Lambda \pm 1/2$ are expected to be very small (a hundred keV or less), due to the weak spin dependence[8] of the ΛN residual interaction. Thus we have summed over j_Λ (in our PWA estimates), since the energy splittings between different j_Λ states are small compared to the experimental energy resolution of about 3 MeV.

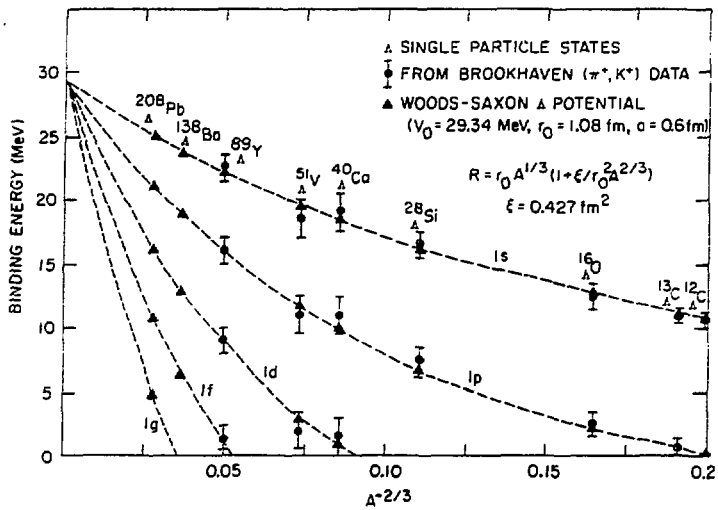

Fig. 6: The binding energies of s_Λ, p_Λ, d_Λ and f_Λ single particle states, as deduced from the data of ref. 3, are plotted as solid circles. The Woods-Saxon binding energies are shown as triangles, using the radius prescription of Eq. 9. If a triangle is not shown, it essentially coincides with the experimental value (solid circle). The parameters of the Λ potential were adjusted to produce a binding of 16 MeV for the $1p_\Lambda$ state in ${}^{89}_{\Lambda}\mathrm{Y}$.

The description of Λ single particle energies can be somewhat improved by including the range of the ΛN potential in the prescription for the radius R of the Λ potential well. Using the relation $<r^2>_V = <r^2>_\rho + <r^2>_{\Lambda N}$ from the folding model, we can write (for $A \geq 12$) the expansion

$$R = r_0 A^{1/3} \left(1 + \xi \left(r_0 A^{1/3}\right)^{-2}\right) \tag{9}$$

where $\xi = 5/6 < r^2 >_{\Lambda N}$. For $V_0 = 29.34$ MeV, $r_0 = 1.08$ fm, $a = 0.6$ fm, $\xi = 0.427$ fm^2, we obtain the fit to the Λ single particle energies shown in Fig. 6. This value of ξ corresponds to $< r^2 >^{1/2}_{\Lambda N} \approx 0.72$ fm $\approx (2m_\pi)^{-1}$, which is reasonable. The predictions are seen to lie within the experimental error bars for all measured hypernuclear systems with $A \geq 12$. On an expanded scale, we

display the $1s_\Lambda - 1p_\Lambda$ and $1p_\Lambda - 1d_\Lambda$ energy splittings Δ_{sp} and Δ_{pd} in Fig. 7, as a function of $A^{-2/3}$. The Woods-Saxon energy splittings are seen to be in excellent agreement with the data, although the predicted Δ_{sp} values may be somewhat too large for intermediate A values.

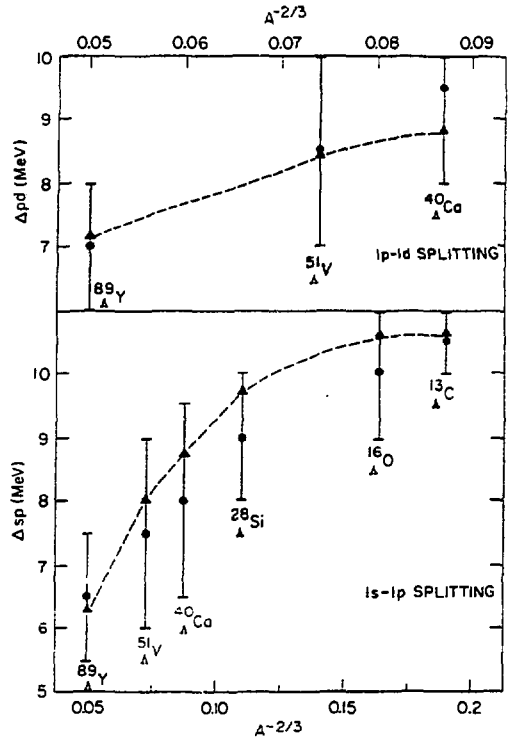

Fig. 7: Level spacing $\Delta_{sp} = |B_\Lambda(1s) - B_\Lambda(1p)|$ and $\Delta_{pd} = |B_\Lambda(1p) - B_\Lambda(1d)|$ as a function of $A^{-2/3}$. The solid circles are deduced from the (π^+, K^+) data of Chrien et al[3], while the solid triangles represent the predictions for the Woods-Saxon Λ potential of Eq. (8), with the radius R given by Eq. (9) and the same parameters as in Fig. 6.

1.3 The Λ in the Nuclear Medium: Distinguishable or Indistinguishable?

The quark configuration of the Λ is $s\,(ud)_{I=0}$. Thus, although the Λ is distinguishable from a nucleon at the hadron level, this is no longer true at the constituent (i.e., quark) level. As the Λ becomes more deeply bound, its wave function becomes more concentrated in the nuclear interior, and one might anticipate some degree of "Pauli pressure" due to the indistinguishability of the non-strange quarks in the Λ. In a very dense medium (which a nucleus is not!), the s quark in the Λ

would be deconfined, and hence no longer localized in a Λ-like three-quark cluster. There have been some theoretical speculations[9–12] concerning the influence of quark degrees of freedom on Λ binding energies. Other possible signatures[13] include magnetic moments of hypernuclei, weak decay branching ratios, and nucleon emission widths for hypernuclear states of $s_\Lambda s_N^{-1}$ structure.

It is very likely that the ground state of a hypernucleus (or a low-lying excited state) is much closer to the limit of a system of color singlet spatially localized three-quark clusters than to the extreme case of a deconfined quark gas. Nevertheless, it is important to search for constraints on the degree of strange quark delocalization. The (π^+, K^+) data are particularly relevant in this regard, since one can study the A dependence of absolute Λ binding energies and level splittings as the levels evolve from the weak to strong binding limits.

It is clear from Figs. 5, 6, and 7 that Λ binding energies agree well with the predictions of a Woods-Saxon potential with a depth V_0 which is independent of A and ℓ_Λ. This is consistent with the picture of the Λ as a distinguishable particle. If a "Pauli repulsion" effect is present, through a Fock-type correction to $V_\Lambda(r)$, the effective V_0 will depend on A as well as the single particle quantum numbers. This is the case if one analyzes the systematics of nucleon single particle binding energies[14].

It is useful to understand the A dependence of B_Λ values in terms of approximate analytic formulae. For a square well of radius $R = r_0 A^{1/3}$ and depth V_0, the binding energy B_Λ of the $1s$ state can be expanded in a Taylor series in powers of $A^{-1/3}$. One finds[15–18]

$$B_\Lambda \approx V_0 \left(1 - \left(\frac{\pi x}{A^{1/3}}\right)^2 \Big/ \left(1 + x^2\right)\right)$$
$$\approx V_0 - \pi^2 \Big/ 2 m_\Lambda r_0^2 A^{2/3} + \cdots \qquad (10)$$

where $x^{-1} = (2\mu_\Lambda V_0)^{1/2} r_0$, $\mu_\Lambda = m_\Lambda (1 + m_\Lambda / A m_N)^{-1}$, and we have set $\hbar = 1$. We see that the series expansion of B_Λ involves two parameters x and $\pi x / A^{1/3}$. If the Λ potential were very deep (large V_0), x would be small, and the series expansion would converge rapidly, even for relatively small A. However, this is not the case in a realistic situation: for $V_0 = 30$ MeV, $r_0 = 1.1$ fm, we obtain $x = 1.44$. Thus $\pi x / A^{1/3}$ remains larger than unity for $A < 100$, and the series expansion only converges for $A > 200$ or so, beyond the mass region where measurements have been made. This explains the fact that the dotted curves in Figs. 5 and 6 are not linear as a function of $A^{-2/3}$. One also notes that an erroneous value of V_0 will be

obtained if one forces an $A^{-2/3}$ fit to the data for $A \leq 90$ and extrapolates to very large A. The results for a Woods-Saxon potential exhibit an A-dependence very close to that of the square well, since $r_0 A^{1/3}$ is large compared to the diffuseness $a \approx 0.6$ fm for the systems of interest.

Similarly, one can derive simple expressions for the level spacings in a square well. One finds for large $A^{1/3}$ the results

$$\Delta_{sp} \approx \Delta_0 \left[\left(\frac{x_1}{\pi} \right)^2 - 1 \right] A^{-2/3}$$
$$\Delta_{pd} \approx \Delta_0 \left[\left(\frac{x_2}{\pi} \right)^2 - \left(\frac{x_1}{\pi} \right)^2 \right] A^{-2/3} \qquad (11)$$

where $\Delta_0 = \pi^2 / 2 m_\Lambda r_0^2 \approx 142$ MeV for $r_0 = 1.1$ fm, and the x_ℓ are the first zeros of the spherical Bessel functions $j_\ell(x)$. As for $B_\Lambda(1s)$, these expressions work well only for $A > 200$. Daskaloyannis et al[17] have derived an expression for $\hbar\omega_\Lambda$ (here identified as Δ_{sp}) which includes higher order terms. They use the approximation $x_1 \approx \pi \left[9/\left(\pi^2 - 3/2\right) + 1 \right]^{1/2} \approx 4.526$, which is quite good. Their result may be recast in the form

$$\Delta_{sp} \approx \frac{3}{2 m_\Lambda} \left(\frac{1}{3} - \frac{1}{2\pi^2} \right)^{-1} \frac{1}{\left(r_0 \tilde{A}^{1/3} \right)^2} \left(1 + \frac{x'}{\tilde{A}^{1/3}} + \xi \left(\frac{x'}{\tilde{A}^{1/3}} \right)^3 \right)^{-2} \qquad (12)$$

where $x' = \left(2 m_\Lambda V_0\right)^{-1/2} / r_0$, $\tilde{A}^{1/3} = \left(\mu_\Lambda / m_\Lambda\right)^{1/2} A^{1/3}$, and $\xi = \pi^2 \left(1 + 2\pi^2\right) / 2\left(2\pi^2 - 3\right) \approx 6.114$. Equation (12) provides an approximation which reproduces the Woods-Saxon results of Figs. 5 and 6 to 10-15% for ${}^{28}_{\Lambda}$Si and heavier systems.

The above formulae show explicitly that the leading term in the sp or pd level spacings varies as $A^{-2/3}$, i.e., as R^{-2}, for large A. However, we have also indicated that the corrections to the leading term of Eq. (11) are sizable for $A < 90$, where data are available. Thus, the curvature in the Δ_{sp} and Δ_{pd} plots of Fig. 7, due to the effect of higher order corrections to the leading $A^{-2/3}$ behavior, is expected. There seems to be good evidence for this curvature in the Δ_{sp} data.

At this point, one is tempted to conclude that the Λ behaves as a distinguishable particle in a hypernucleus. The experimentally observed Λ single particle states remain sharply defined even when their binding exceeds 20 MeV, unlike deeply bound nucleon single particle orbits, which acquire a large spreading width. Even when the Λ sits in the center of a heavy nucleus, it is still in a relatively low density environment, and one does not expect large shifts in binding due to non-strange quark antisymmetrization. No quantitative estimates of the change in

$B_\Lambda(1s)$, Δ_{sp} or Δ_{pd} due to quark effects are available. Such estimates should be done.

For nucleon single particle spacings, one expects a leading term proportional to $A^{-1/3}$ rather than $A^{-2/3}$. Daskaloyannis et al[17] obtain a formula for the oscillator spacing $\hbar\omega_N$ ($\sim \Delta_{sp}$) of the form

$$\hbar\omega_N = \frac{5}{4}\left(\frac{3}{2}\right)^{1/3}\left(\frac{\hbar}{m_N r_0^2}\right)A^{-1/3}\left(1-\alpha A^{-2/3}+\beta A^{-4/3}+\ldots\right). \qquad (13)$$

Numerically, they find[17]

$$\hbar\omega_N \approx 39A^{-1/3} - 23A^{-1}. \qquad (14)$$

In more detail, $\hbar\omega_N$ depends on the number of valence nucleons n as well as A. This leads to characteristic discontinuities in the slope of $\hbar\omega_N$ at the closed shells[17]. This effect is observed for nucleons, and it would be interesting to look for similar discontinuities with Λ's.

For a distinguishable Λ, the corrections to the $A^{-2/3}$ dependence of Δ_{sp} are of order A^{-1}. Quark effects would contribute a term which varies as $A^{-1/3}$, and for sufficiently large A one could in principle distinguish such a term from an A^{-1} correction. This seems difficult to do with the present (π^+, K^+) data, since one is in a regime ($A < 90$) where series expansions in powers of $A^{-1/3}$ are only slowly convergent.

It is amusing to note that one could parametrize the data on Δ_{sp} in Fig. 7 in a form in which the leading term varies as $A^{-1/3}$, i.e.

$$\Delta_{sp} \approx 39A^{-1/3} - 36A^{-2/3}. \qquad (15)$$

This bears a strong resemblance to the formula (14) for an indistinguishable baryon! Clearly, one needs data on $A > 100$ hypernuclei in order to choose between these alternatives. For $^{208}_{\Lambda}$Pb, we predict

$$\Delta_{sp} \approx \begin{cases} 4.1 \text{ MeV (Fig.6)} \\ 5.6 \text{ MeV (Eq. (15))} \end{cases} \qquad (16)$$

This difference of Δ_{sp} values of 1.5 MeV is rather sizable, and a ^{208}Pb (π^+, K^+) $^{208}_{\Lambda}$Pb experiment could settle this important point. In the PWA, we predict a cross section for the $\left(_\Lambda s_{1/2} \times i^{-1}_{13/2}\right)_{6^+}$ state in $^{208}_{\Lambda}$Pb of

$$\left(\frac{d\sigma}{d\Omega}\right) \approx \begin{cases} 3.7\mu b/sr \text{ at } 1.05 \text{ GeV/c} \\ 1.9\mu b/sr \text{ at } 1.5 \text{ GeV/c} \end{cases} \qquad (17)$$

The $\Delta L = 6$ transition is somewhat better matched kinematically at 1.5 GeV/c, but the $\pi^+ n \rightarrow K^+ \Lambda$ cross section has dropped considerably with respect to its peak value of about $400\,\mu b/sr$ at 1.05 GeV/c. Even allowing for a factor of 10-20 or so for absorption effects, the resulting cross section of 0.2-0.4 $\mu b/sr$ at 1.05 GeV/c is still measurable at the Brookhaven AGS.

2. KAON-NUCLEUS SCATTERING

The two-body K^+N cross section is rather small ($\sim$ 10 mb) at low momentum ($\leq$ 500MeV/c), and hence the K^+ should be a sensitive probe of neutron/proton densities ρ_n and ρ_p, since the first order approximation $V \sim \rho_n t_{K+n} + \rho_p t_{K+p}$ should be very good, with small and calculable higher order corrections. The K^+ as a "weakly" interacting hadronic probe thus occupies a unique position[19].

The first significant tests of these ideas came after measurements[20] of K^+ elastic scattering from ^{12}C and ^{40}Ca at 800 MeV/c. Although the first order optical potential provided an acceptable fit to the ^{40}Ca data, the theoretical predictions for $K^+ + {}^{12}$C elastic scattering, using the free space K^+N amplitudes of Martin[21], fell short of the data. The same difficulty appears in the total cross section for $K^+ + {}^{12}$C.

Although first order multiple scattering theory agrees very well with the data[22] above 1.2 GeV/c, where the K^+N amplitudes involve several partial waves (s, p, d, f) and the K^+N cross section is of normal hadronic size, the theory falls consistently below the data at lower momentum. Equivalently, the theory predicts substantial "shadowing" in the 0.7 to 1 GeV/c region, whereas the total cross section $\left(\sigma^T\right)$ data for $K^+ + {}^{12}$C lie close to $6 \times \sigma^T_{K+d}$, i.e., no shadowing.

A way to account for the discrepancy between multiple scattering theory and data for $K^+ + {}^{12}$C was suggested by Siegel et al[23]. They argue, in analogy to one interpretation of the EMC effect, that a nucleon in a nucleus is "swollen," and hence the S_{11} K^+ nucleon phase shift δ, which in free space is well parametrized by

$$\delta\left(S_{11}\right) = -kR\,, \tag{18}$$

where $R \approx 0.32$ fm is an effective hard sphere radius, is modified to $\delta\left(S_{11}\right) = -k\tilde{R}$, where $\tilde{R} > R$, in the nucleus. They find that an increase of $\delta\left(S_{11}\right)$ by 15% $\left(\tilde{R}/R = 1.15\right)$, consistent with an increase of confinement scale of 10-30%, produces agreement with the $K^+ + {}^{12}$C data. Note that below 500 MeV/c, the S_{11} phase shift dominates the K^+N interaction. At higher momentum, the P-wave

cross section grows rapidly (perhaps reflecting exotic Z^* resonances), and the K^+ interaction becomes more absorptive.

The idea of testing partial deconfinement by K^+ nucleus scattering is attractive, but of course there may also be a more conventional explanation of the discrepancies in the $K^+ + {}^{12}C$ data. The advantage of the K^+ over other hadronic probes is that $< \sigma >$ is relatively small (long mean free path), and hence the multiple scattering expansion converges rapidly.

For a strongly absorbed probe, such as a $\pi^{\pm}$ or K^-, the large multiple scattering corrections mask the subtle changes due to small variations of confinement scale in the nucleus. The K^+, on the other hand, interacts with nucleons to leading order much as a virtual photon does. This analogy is illustrated in Fig. 8(a,b). In a boson exchange picture, the $\{\rho^0, w\}$ vector mesons dominate, since single pion exchange is absent. For the K^+, unlike the (e, e') case, there are higher order processes (Fig. 8(c,d)) involving K^*N, $K^*\Delta$ and $K\Delta$ intermediate states. These play an important role in driving possible Z^* resonance formation.

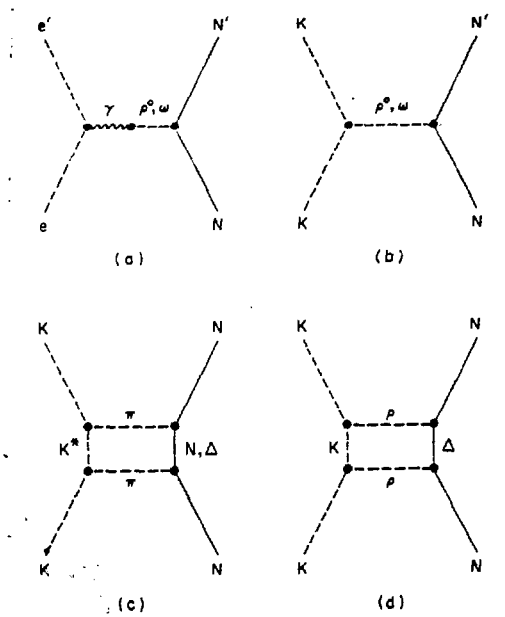

Fig. 8: The interaction via vector meson exchange of virtual photons and kaons with nucleons is shown in a and b. Additional higher order processes which occur for the kaon are displayed in c and d.

In $(e,e'p)$, the data on transverse and longitudinal form factors have been interpreted as indicating an increased charge radius and magnetic moment for a nucleon immersed in the nuclear medium[24]. At 800 MeV/c, the $\left(K^+, K^{+'}N\right)$ quasielastic process dominates the K^+ elastic scattering[20], so the changes in the nucleon purportedly seen in $(e,e'p)$ should also be discernible for K^+. In the medium, the meson clouds of nucleons are modified, and this implies a density dependent change in the effective mass m^* of exchanged mesons in Figs. 8(b-d). One expects that $m^* < m$, where m is the mass in free space; this will lead to a K^+N S_{11} phase shift which exhibits increased repulsion ($\tilde{R} > R$ in Eq. (18)), in the direction of improving the fit to the $K^+ + {}^{12}$C data. In addition, there will be additional corrections of "exchange current" type, where the K^+ interacts a pion in flight between two nucleons. Note that $K\pi \rightarrow K\pi$ scattering is a resonant (non-exotic) process, so such processes could be significant. The box diagrams of Figs. 8(c,d) will also experience density dependent modifications in the nucleus. The real part of Fig. 8(c), for instance, is rapidly energy-dependent around 600-800 MeV/c, near the K^*N threshold. The modification of this energy dependence due to the medium corrections could be important, since the effective threshold is shifted. The quantitative aspects of these different mechanisms are under study[25].

Very recently[26], $K^+ + {}^{12}$C and $K^+ + d$ total cross sections were measured at the Brookhaven AGS in the momentum range 550-800 MeV/c. At the lower momentum, one is still dominated by s-wave K^+N interactions, and the elementary K^+N cross section is very small. This is a favorable regime for looking at subtle changes of nucleon structure in the nucleus. The experimental data[26] are currently under analysis.

ACKNOWLEDGEMENTS

Thanks are due to Bob Chrien and Phil Pile for extensive discussions of the Brookhaven (π^+, K^+) data and to John Millener for cogent observations on theoretical questions.

REFERENCES

1. Proceedings of the International Symposium on Hypernuclear and Kaon Physics, Brookhaven, September 1985, ed. R. E. Chrien, Nucl. Phys. A450, 1c-586c (1986).
2. Proceedings of the 1986 INS International Symposium on Hypernuclear Physics, eds. H. Bando, O. Hashimoto and K. Ogawa, Institute for Nuclear Study, University of Tokyo (1986), pp. 1-448.

3. Chrien, R. E. et al. "Studies of hypernuclei by associated production", BNL 39722, to be published in Proceedings of the XI International Conference on Particles and Nuclei (PANIC), Kyoto, Japan, April 1987.
4. Dover, C. B., L. Ludeking and G. E. Walker, Phys. Rev. C22, 2073 (1980).
5. Bando, H. and T. Motoba, Prog. Theor. Phys. 76, No. 6 (1986); H. Bando, T. Motoba and J. Zofka, in Abstract Book II, PANIC (1987), pp. 564-565.
6. Milner, C. et al, Phys. Rev. Lett. 54, 102 (1985).
7. Bohr, A. and B. Mottelson, "Nuclear Structure", Vol. I, W. A. Benjamin, Inc., New York (1969).
8. Millener, D. J., A. Gal, C. B. Dover and R. H. Dalitz, Phys. Rev. C31, 499 (1985).
9. Hungerford, E. V. and L. C. Biedenharn, Phys. Lett. 142B , 232 (1984).
10. Goldman, T., Proc. 1st Conf. on Intersections Between Particle and Nuclear Physics, ed. R. E. Mischke, American Institute of Physics, New York (1984) pp. 799-805.
11. Gibson, B. F., Proc. Conf. on Hadronic Probes and Nuclear Interactions, eds. J. R. Comfort et al, American Institute of Physics, New York (1985) pp. 390-391.
12. Takeuchi, S. and K. Shimizu, Tokyo preprint (1985).
13. Dover, C. B., Proc. International Nuclear Physics Conf., Harrogate, England, Inst. Phys. Conf. Ser. No. 86, IOP Publishing Ltd (1987) pp. 99-118.
14. Millener, D. J. and P. E. Hodgson, Nucl. Phys. A209, 59 (1973).
15. Gal. A., in Advances in Nuclear Physics, eds. M. Baranger and E. Vogt, Plenum Press, New York (1975), Vol. 8, pp. 1-120.
16. Auerbach, N. and A. Gal, Phys. Lett. 48B, 22 (1974).
17. Daskaloyannis, C. B. et al, Phys. Lett. 121B, 91 (1983) and 134B, 147 (1984).
18. Grypeos, M. E. and C. G. Koutroulos, Nucl. Phys. A450, 307c (1986).
19. Dover, C. B. and P. J. Moffa, Phys. Rev. C16, 1087 (1977).
20. Marlow, D. et al, Phys. Rev. C25, 2619 (1982) and C30, 1662 (1984).
21. Martin, B. R., Nucl. Phys. B94, 413 (1975).
22. Bugg, D. et al, Phys. Rev. 168, 1466 (1968).
23. Siegel, P. B., W. B. Kaufmann and W. R. Gibbs, Phys. Rev. C30, 1256 (1984) and C31, 2184 (1985).
24. Noble, J. V., Phys. Rev. Lett. 46, 412 (1981); Mulders, P. J., Phys. Rev. Lett. 54, 2560 (1985).
25. Brown, G. E., C. B. Dover and K. Kubodera, work in progress.
26. Alster J. et al, Brookhaven AGS Experiment 835.